Identification of low–frequency magnetosheath waves

Richard E. Denton, Marc R. Lessard, and James W. LaBelle

Physics and Astronomy Department, Dartmouth College, Hanover, New Hampshire

S. Peter Gary

Los Alamos National Laboratory, Los Alamos, New Mexico.

Abstract. Four low-frequency modes may propagate in a high-beta, nearly bi-Maxwellian plasma, the magnetosonic, Alfvén, ion acoustic, and mirror modes. This study uses a procedure based on linear Vlasov theory for the identification of these modes by use of transport ratios, dimensionless ratios of the fluctuating field and plasma quantities. A single parameter, the mode deviation, is calculated which characterizes the difference between the theoretical transport ratios of a particular mode and the observed ratios. As well as determining the mode that best describes the observed fluctuations, it gives us a measure of whether or not the resulting identification is unique. Unfortunately, a unique identification is not always possible because of problems discussed herein. One problem is that the parallel phase ratio (related to the phase angle between density and parallel magnetic fluctuations) is often not well defined. Using the plasma and magnetic field data gathered by the Active Magnetospheric Particle Tracer Explorers/Ion Release Module spacecraft, we calculate the mode deviations and identify the modes observed in the magnetosheath. The quasi-perpendicular (with wave vector at a large angle to the background magnetic field) mirror mode is clearly identified in the inner (close to the magnetopause) and middle magnetosheath. The quasi-parallel mirror mode may be observed in the inner magnetosheath, but that identification is not certain. Alfvén-like modes are observed for one event in the outer magnetosheath (near the bow shock) and are probably observed in two others.

1. Introduction

Besides their inherent interest, low-frequency waves with angular frequency ω below the proton gyrofrequency Ω_p are important both because they can modify the background plasma (for instance, the temperature anisotropy) and because they can be used to diagnose plasma properties. The first step in the study of such waves is their identification. One possible means of identification is the use of transport ratios, dimensionless ratios of the fluctuating field and plasma quantities (see the review by *Schwartz et al.* [1996]). While various schemes have been used to distinguish different types of waves, the first systematic scheme designed to distinguish all types of low-frequency waves was that of *Song et al.* [1994]. *Denton et al.* [1995] described another scheme (similar to that described by *Song et al.* [1994, Appendix B]). Differences in Denton et al.'s approach involved the use of kinetic theory rather than MHD, the attribution of equal weight to the information from dif-

ferent transport ratios rather than a decision tree, the use of the Alfvén ratio rather than Song et al.'s Doppler ratio, and allowance for the possibility of modes such as the quasi-parallel (wave vector **k** approximately parallel to the background magnetic field **B**₀) mirror and ion acoustic modes. (See *Schwartz et al.* [1996] for a discussion of the different methods.). *Denton et al.* [1995] compared theoretical values of the transport ratios with those calculated using observations from the Active Magnetospheric Particle Tracer Explorers/Ion Release Module (AMPTE/IRM) during times in which the spacecraft was in the terrestrial magnetosheath, close to magnetopause. Waves in that region were best identified as the quasi-perpendicular (**k** approximately perpendicular to **B**₀) mirror mode. A few of the events were best described by the quasi-parallel mirror mode, but this identification was somewhat problematic, since it was not understood how quasi-parallel mirror modes might be generated.

Several studies attempting to identify low-frequency waves ought to be mentioned. *Gleaves and Southwood* [1990, 1991] compare measured and theoretical frequencies to identify Alfvén and slow waves (we might dispute this identification) in the afternoon magnetosheath. *Lacombe et al.* [1995] examine two very quiet intervals in

the extended magnetosheath (during periods of low dynamic pressure). These intervals were unusual in that the phase difference between magnetic fluctuations parallel to the magnetic field and the density fluctuations was well-defined even though these fluctuations were small. (The problems associated with measurement of this phase angle are discussed in detail in this paper.) Lacombe et al. identified some waves as the Alfvén ion cyclotron wave (our Alfvén wave) and explained other waves as being a mixed mode with properties of the Alfvén ion cyclotron wave and He^{2+} cut-off mode [see *Denton et al.*, 1994]. These waves are at higher frequency than the ones considered in this paper (for our events, $\omega \ll \Omega_p$). *Blanco-Cano and Schwartz* [1997] identify left- and right-hand polarized Alfvénic waves in the ion foreshock. All of these authors make heavy use of polarization information, including the use of the direction of the magnetic minimum variance direction, to determine the direction of the wave vector $\mathbf{k}$. We prefer not to emphasize the results of such an analysis, since superposition of waves can make the direction of $\mathbf{k}$ difficult or impossible to determine [*Denton et al.*, 1996]. However, *Lacombe et al.* [1995] do seem to have been careful in their use of the minimum variance direction. They claim that the orientation of the magnetic fluctuations is constant with respect to $\mathbf{B}_0$ over a number of subintervals. Such constancy would suggest that the direction of $\mathbf{k}$ is adequately determined [see *Denton et al.*, 1996]. A major difference between our work and that of these authors is that we attempt to lay out a systematic procedure for the identification of observed waves. This is not easy to do, as some of our results indicate.

In this paper, we extend the study of *Denton et al.* [1995] to examine the waves in the middle and outer magnetosheath (close to the bow shock). In brief, we compare the observed wave properties (transport ratios) to those calculated using infinite homogeneous linear kinetic theory in order to identify the waves. We also reexamine two of the inner magnetosheath (close to the magnetopause) events that were previously identified as the quasi-parallel mirror mode [*Denton et al.*, 1995]. In section 2, we review the wave identification method of *Denton et al.* [1995] and explain the modifications in technique we make here. In section 3, we describe our new data set, and in section 4, we apply our method to identify the waves. Section 5 is a discussion section, while section 6 presents our conclusions. While the method always yields a mode that best fits the observations, in some cases, the identification is not unique, particularly when the fluctuations are quasi-parallel. Difficulties are discussed, including the fact that it is often difficult to measure the parallel phase ratio (related to the phase angle between density and parallel magnetic fluctuations).

2. Theory and Method

2.1. Low-Frequency Modes

At frequency $f \ll F_{cp}$, where F_{cp} is the proton cyclotron frequency, up to four distinct modes can propagate in a relatively isotropic plasma: the three waves corresponding to the normal modes of MHD theory and a fourth zero-frequency mode. At low $\beta_{\|p}$ (proton beta calculated using the temperature associated with motion along $\mathbf{B}_0$), a simple description of the finite frequency modes as "slow," "intermediate," and "fast," corresponding to our ion acoustic, Alfvén, and magnetosonic modes, respectively, is adequate. However, at large $\beta_{\|p}$ the order of phase speeds changes as the dispersion surfaces cross each other. For that reason, we categorize the wave modes based on physical properties (similar transport ratios) rather than phase speed. See [*Krauss-Varban et al.*, 1994] for plots of dispersion surfaces of the finite frequency modes. Our ion acoustic, Alfvén, and magnetosonic modes are the same as the "slow/sound," "Alfvén/ion cyclotron," and "fast/magnetosonic" modes of *Krauss-Varban et al.* [1994]. For each of our modes, we distinguish "quasi-parallel" and "quasi-perpendicular" regimes refering approximately to $5° < \theta_{kB} \lesssim 20°$ and $60° \lesssim \theta_{kB} < 85°$, respectively, where θ_{kB} represents the angle between $\mathbf{k}$ and $\mathbf{B}_0$. Kinetic theory predicts the existence of a fourth zero-frequency mode, the mirror mode [*Tajiri*, 1967]. Taking into account the four basic waves and two θ_{kB} regimes, we consider there to be eight different modes.

The angular range for our quasi-parallel modes represents the first difference between the present method and that of *Denton et al.* [1995]. Our parallel modes have $\mathbf{k}$ up to 20° off the direction of $\mathbf{B}_0$, whereas theirs could be as much as 30° off. The reason for this change is that the modes have a much better defined set of properties for angles up to only 20°. Beyond that, the mode properties become more similar to those of the quasi-perpendicular modes. Rather than defining the quasi-parallel modes so that their ranges of theoretical values encompass those of the quasi-perpendicular modes, we felt that it was better to define the quasi-parallel modes more narrowly. If an observed mode has properties between that of the quasi-parallel and quasi-perpendicular mode, it may well indicate that the mode is at one of the intermediate angles between 20° and 60°.

2.2. Definition of Transport Ratios

Gary and Winske [1992] and *Gary* [1992] introduced the term "transport ratios" to denote dimensionless ratios of the squares of fluctuating field and plasma quantities. These authors, as well as *Lacombe et al.* [1990, 1992], *Belmont et al.* [1992], *Anderson et al.* [1994],

Song et al. [1994], and *Denton et al.* [1995], have used different combinations of such ratios to identify low-frequency fluctuations in the magnetosheath. We use a somewhat modified version of the method used by *Denton et al.* [1995]. We use both plasma and magnetic field observations for our database as well as Vlasov theory for the computation of the transport ratios.

Following *Gary and Winske* [1992], we use the notation $\langle ab \rangle_{k\omega}$ to indicate the correlation between a and b, which is a function of $\mathbf{k}$ and ω. We estimate this quantity from the observed finite length discrete time series by first taking the discrete time Fourier transforms of a and b and then computing the product $a_\omega b_\omega^*$, where b_ω^* is the complex conjugate of b_ω.

We base our identification procedure on the following transport ratios (see *Denton et al.* [1995] for references): the compressibility of the jth species

$$C_j(\mathbf{k}, \omega) \equiv \frac{\langle \delta n_j \delta n_j \rangle_{k\omega}}{n_j^2} \frac{B_0^2}{\langle \delta \mathbf{B} \cdot \delta \mathbf{B} \rangle_{k\omega}} , \qquad (1)$$

the Alfvén ratio of the jth species

$$R_{Aj}(\mathbf{k}, \omega) \equiv \frac{\langle \delta \mathbf{v}_j \cdot \delta \mathbf{v}_j \rangle_{k\omega}}{V_A^2} \frac{B_0^2}{\langle \delta \mathbf{B} \cdot \delta \mathbf{B} \rangle_{k\omega}} , \qquad (2)$$

where $V_A \equiv B_0/\sqrt{4\pi n_p m_p}$ is the Alfvén speed, the parallel phase ratio

$$R_{\|n_j}(\mathbf{k}, \omega) \equiv \frac{\langle \delta n_j \delta B_\| \rangle_{k\omega}}{\sqrt{\langle \delta n_j \delta n_j \rangle_{k\omega} \langle \delta B_\| \delta B_\| \rangle_{k\omega}}} , \qquad (3)$$

which is equivalent to the cosine of the phase angle between $\delta B_\|$ and δn_j, and the magnetic compressibility

$$C_B(\mathbf{k}, \omega) \equiv \frac{\langle \delta B_\| \delta B_\| \rangle_{k\omega}}{\langle \delta \mathbf{B} \cdot \delta \mathbf{B} \rangle_{k\omega}} . \qquad (4)$$

The magnetic compressibility C_B is functionally equivalent to the transverse ratio of *Song et al.* [1994].

As mentioned in section 1, superposition of waves can make the direction of $\mathbf{k}$ difficult or impossible to determine [*Denton et al.*, 1996]. Because of this, we do not make use of the noncoplanar ratio (discussed by *Denton et al.* [1995] but not used; this quantity depends on the direction of the wave vector $\mathbf{k}$). (For quasi-monochromatic superposed waves, the wave angle between $\mathbf{k}$ and $\mathbf{B}_0$ can sometimes be inferred from the statistical properties of the waves [*Denton et al.*, 1996], but the waves we are studying here are usually broadband.)

In two cases, we mention values of the cross helicity σ_{cj} [*Gary and Winske*, 1992]

$$\sigma_{cj} \equiv \frac{2\langle \delta \mathbf{v}_j \cdot \delta \mathbf{B} \rangle_{k\omega}/(V_A B_0)}{\frac{\langle \delta \mathbf{v}_j \cdot \delta \mathbf{v}_j \rangle_{k\omega}}{V_A^2} + \frac{\langle \delta \mathbf{B} \cdot \delta \mathbf{B} \rangle_{k\omega}}{B_0^2}} . \qquad (5)$$

For a single wave (one $\mathbf{k}$), this quantity is very helpful for distinguishing the mirror mode from an Alfvén wave. Its value for the mirror mode should be about zero, while for an Alfvén wave its value should be about ± 1, depending on the direction of $\mathbf{k}$ relative to $\mathbf{B}_0$. Unfortunately, its significance is blurred when there is a superposition of waves. A superposition of two Alfvén waves propagating in opposite directions will also lead to zero value for σ_{cj}. Because of this, the value of σ_{cj} will only be helpful if its magnitude is large (appreciable compared to unity). Such a result would favor an identification as an Alfvén wave (propagating mainly in one direction) rather than that of a mirror mode.

We estimate the transport ratios from the finite time series of measured ion moments (assumed to be protons; hence we use the subscript p) and magnetic field. Low frequencies are neglected owing to the finite length of the time series, and high frequencies ($f > 0.04$ Hz) are neglected to avoid certain difficulties due to uneven data sampling. (By averaging together five spin periods of AMPTE/IRM plasma moment data, evenly sampled time series may be achieved.) Transport ratios are useful as identifiers of low-frequency fluctuations, primarily because they can all be computed in the same way from observed field and plasma fluctuation spectra as well as from linear Vlasov theory. We have chosen these particular transport ratios because each one provides independent information and does not change its value under a change of reference frame [*Denton et al.*, 1995]. An example event showing measured values of our transport ratios versus frequency is presented in Figure 1.

2.3. Theoretical Values of Transport Ratios

We have computed the transport ratios defined above through the use of a linear Vlasov dispersion code for $\beta_{\|p} = 0.10$, $\beta_{\|p} = 1.0$, and $\beta_{\|p} = 10.0$ using bi-Maxwellian, zeroth-order distribution functions [*Gary*, 1992]. A single pure mode in an infinitely homogeneous plasma is assumed. Other parameters are $T_e = T_{\|p}/4$, $(T_\perp/T_\|)_p = 1 + 0.65\beta_{\|p}^{-0.40}$, and $kc/\omega_p = 0.10$, where k is the wave number, c is the speed of light, and $\omega_p \equiv \sqrt{4\pi n_p e^2/m_p}$ is the plasma frequency. The formula for $(T_\perp/T_\|)_p$ is from *Gary et al.* [1994, equation (3c)]. It is particularly appropriate for the magnetosheath but is also a rough upper limit appropriate for any proton/electron plasma. Values of the transport ratios are listed in Table 1, where quasi-perpendicular and quasi-parallel modes are considered to be separate modes. In Table 1, which replaces Table 2b of *Denton et al.* [1995], the notation $[a, b]$ indicates that the value is a at the lower limit of the angular range and is b at the upper limit. We have dropped variations of less than 10% in order to keep Table 1 as simple as possible. (For ratio-mapped quantities, discussed below, we have
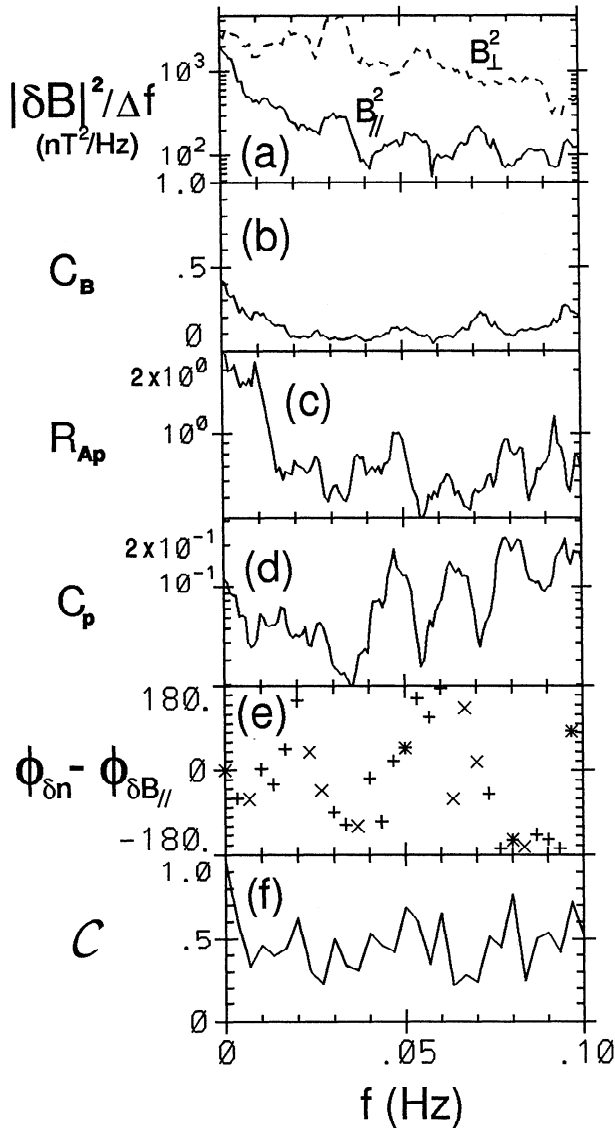
Figure 1. (a) Power spectra $|\delta B|^2/\Delta f$ (nT^2/Hz) of magnetic fluctuations parallel (solid curve) and perpendicular (dashed curve) to $\mathbf{B}_0$, (b) magnetic compressibility C_B, (c) Alfvén ratio R_{Ap}, (d) compressibility C_p, (e) phase angle $\phi_{\delta n} - \phi_{\delta B_{//}}$, and (f) phase angle coherence C versus frequency in hertz for the November 12, 1984, event (event 5 in Table 2a). In Figure 1e, asterisks denote frequencies with $2/3 \leq C \leq 1$, pluses are for $1/3 \leq C < 2/3$, and crosses are for $0 \leq C < 1/3$. $F_{cp} = 0.26$ Hz.

actually dropped 10% variations of the ratio mapped values.) The value 100 is typically used to indicate a large number. Our procedure for mode identification consists of comparing the observed transport ratios for a particular fluctuation with those of Table 1. Put most simply, the mode that best matches the observations is identified as the most likely description of the observed fluctuations.

Values of frequency and growth rate for the theoretical modes are given by Denton et al. [1995, Table 2a]. These must be applied with caution, since there might

be nonlinear sources of waves not accounted for by infinite homogeneous theory. Here we do not take these into account and simply try to identify the waves based on the transport ratios.

Two of our transport ratios, R_{Ap} and C_p, are defined as the ratio of two totally independent quantities and have values that can vary between zero and infinity. We map the possibly infinite variations of these quantities to range 0–2 according to the following ratio mapping $\mathcal{M}$ of the quantity q

$$\begin{aligned}\mathcal{M}(q) &= q, & q \leq 1 \\ \mathcal{M}(q) &= 2 - \tfrac{1}{q}, & q > 1.\end{aligned} \qquad (6)$$

We use $\mathcal{M}(R_{Ap})$ and $\mathcal{M}(C_B)$ rather than R_{Ap} and C_B to get a measure of the difference of observed and theoretical values for these transport ratios. The ratio mapping $\mathcal{M}$ has the property that $|\mathcal{M}(q_1) - \mathcal{M}(q_2)| = |\mathcal{M}(1/q_1) - \mathcal{M}(1/q_2)|$, which is desirable because we could just as well have defined R_{Ap} or C_p as the inverse of their definitions.

Figures 2a–2d display the information of Table 1 pictorially. For each mode there is a range of values for C_B, $\mathcal{M}(R_{Ap})$, $\mathcal{M}(C_p)$, and $R_{\|n_p}$ for three different values of $\beta_{\|p}$. We take the midpoint of each range of a transport ratio to get a point in C_B-$\mathcal{M}(R_{Ap})$-$\mathcal{M}(C_p)$-$R_{\|n_p}$ space for each value of $\beta_{\|p}$ and for each mode. Figures 2a and 2b display points for the five modes with $C_B \leq 0.1$, the $Q-\|$ and $Q-\perp$ Alfvén and the $Q-\|$ magnetosonic, ion acoustic, and mirror modes, whereas Figures 2c and 2d display points for the three modes with $C_B \geq 0.75$, the $Q-\perp$ magnetosonic, ion acoustic, and mirror modes. The values of $\mathcal{M}(R_{Ap})$ are plotted versus $\mathcal{M}(C_p)$ in Figures 2a and 2c, while values of $R_{\|n_p}$ versus $\mathcal{M}(C_p)$ are plotted in Figures 2b and 2d. For each mode, three symbols connected by a dashed line indicate the values of the transport ratios at $\beta_{\|p} = 0.10$, $\beta_{\|p} = 1.0$, and $\beta_{\|p} = 10.0$. The open symbol is for the low $\beta_{\|p} = 0.10$. A single open symbol is plotted if the values of transport ratios overlap at all values of $\beta_{\|p}$. The abbreviation "MgS" and the diamond symbol are used for the magnetosonic mode, "Alf" and the circle symbol denote the Alfvén mode, "IAc" and the upperward pointing triangle symbol represent the ion acoustic mode, and "Mir" and the downward pointing triangle symbol are for the mirror mode. The solid lines represent the theoretical variation with respect to θ_{kB}. Of course, it should be remembered that our method assumes a single linear mode in an infinite homogenous plasma with the parameters specified at the beginning of this section; to include variations on any of these would certainly lead to more theoretical variation.

Using Figure 2, one can readily visualize the differences between the modes. All the quasi-perpendicular $(Q-\perp)$ modes have large C_B except the Alfvén wave. Owing to the fact that the Alfvén wave fluctuates outside the plane of both $\mathbf{B}_0$ and $\mathbf{k}$, both the parallel magnetic and density fluctuations are small. Thus C_B and C_p are small. In terms of the transport ratios used here,

Table 1. Transport Ratios for Proton Beta $\beta_{\|p} = 0.10$, $\beta_{\|p} = 1.0$, and $\beta_{\|p} = 10.0$

$\beta_{\|p}$	Mode	θ_{kB}, deg	C_B	R_{Ap}	C_p	$R_{\|n_p}$
0.10	magnetosonic	[5,20]	[0.,0.1]	1.	0.	1.
		[60,85]	[0.75,1.]	1.25	[0.8,1.]	1.
0.10	Alfvén	[5,20]	0.	1.15	0.	1.
		[65,85]	0.	1.	0.	-1.
0.10	ion acoustic	[5,20]	[0.,0.1]	100.	100.	-1.
		[60,80]	[0.75,1.]	100.	100.	-1.
0.10	mirror	[5,20]	[0.,0.1]	[1.,2.7]	[1.,12.]	-1.
		[60,85]	[0.75,1.]	[0.5,0.2]	9.	-1.
1.0	magnetosonic	[5,20]	[0.,0.1]	[1.2,1.7]	[0.,0.3]	[.8,.9]
		[60,85]	[0.75,1.]	2.7	1.	1.
1.0	Alfvén	[5,20]	0.	1.4	0.	0.75
		[60,85]	0.	1.35	0.	-1.
1.0	ion acoustic	[5,20]	[0.,0.1]	100.	100.	[-0.5,-0.8]
		[60,80]	[0.75,1.]	100.	100.	-1.
1.0	mirror	[5,20]	[0.,0.1]	6.	[0.4,3.0]	-1.
		[60,85]	[0.75,1.]	0.	[0.2,0.4]	-1.
10.0	magnetosonic	[5,20]	[0.,0.1]	[3.9,2.8]	0.	0.
		[60,85]	[0.75,1.]	100.	1.	1.
10.0	Alfvén	[5,20]	0.	2.1	0.	[0.,0.2]
		[60,85]	0.	2.3	0.	-0.45
10.0	ion acoustic	[5,20]	[0.,0.1]	100.	100.	[-0.2,-0.45]
		[60,80]	[0.7,1.]	100.	100.	-1.
10.0	mirror	[5,20]	[0.,0.1]	100.	[0.2,1.7]	-1.
		[60,85]	[0.75,1.]	0.	0.	-1.

Here θ_{kB} is the angle between $\mathbf{k}$ and $\mathbf{B}_0$; C_B is the magnetic compressibility; R_{Ap} is the Alfvén ratio; C_p is the compressibility; $R_{\|n_p}$ is the parallel phase ratio; and $[a,b]$ indicates that the quantity has value a at the low value of θ_{kB} and value b at the high value of θ_{kB}. Parameters assumed are $T_e = T_{\|p}/4$, proton temperature ratio $(T_\perp/T_\|)_p = 1 + 0.65\beta_{\|p}^{-0.40}$, and $kc/\omega_p = 0.10$, where $\mathbf{k}$ is the wave vector, c is the speed of light, and ω_p is the plasma frequency.

the quasi-parallel Alfvén and magnetosonic modes are essentially the same mode. They differ only with respect to the direction of the fluctuating magnetic field in the plane perpendicular to $\mathbf{B}_0$. They both have $R_{Ap} \approx 1$ (exactly 1 for a zero $\beta_{\|p}$ plasma). Where a distinction between these modes is important, one will need to determine the polarization [see Blanco-Cano and Schwartz, 1997]. The quasi-perpendicular magnetosonic mode has C_B and C_p near unity owing to the compressional nature of the mode. The mirror mode, ion acoustic mode, and quasi-perpendicular $(Q-\perp)$ Alfvén wave have density and magnetic fluctuations out of phase, and thus $R_{\|n_p} < 0$; the other modes have $R_{\|n_p} > 0$. In principle, this can be used to distinguish the quasi-parallel and quasi-perpendicular Alfvén modes; however, in practice, $R_{\|n_p}$ is not likely to be well defined for an Alfvén mode with very small density and parallel magnetic fluctuations. (We discuss this issue further in section 2.4.) At $\theta_{kB} = 0$, the ion acoustic mode is purely electrostatic for which $\delta\mathbf{B} = 0$. The ion acoustic mode maintains a predominantly electrostatic character at other values of θ_{kB}, and it can be distinguished by large values of R_{Ap} and C_p. Magnetic fluctuations dominate for the quasi-perpendicular mirror mode which can be distinguished by small values of R_{Ap} and C_p (except at low $\beta_{\|p}$).

2.4. Problems With the Measurement of $R_{\|n_p}$

Recall that the parallel phase ratio $R_{\|n_p}$ is the cosine of the phase angle between the $\delta B_\|$ and δn_p fluctuations. It is possible that the resulting value of $R_{\|n_p}$ may not be well defined for a particular data set. Consider especially the case of Alfvén waves for which $\delta B_\|$ and δn_p are both very small. In that case, the observed $\delta B_\|$ and δn_p may be due to noise, with a relative phase angle that is random.

Denton et al. [1995] calculated $R_{\|n_p}$ using a fast Fourier transform (FFT) over the entire period of observation. Here, in order to get a measure of the significance of $R_{\|n_p}$, we divide the data for each event into N_C data segments. We calculate the complex quantity Q

$$Q = \frac{\sum_{i=1}^{N_c} \delta n_{\omega i}\delta B_{\|\omega i}^*}{\sum_{i=1}^{N_c} |\delta n_{\omega i}||\delta B_{\|\omega i}|}, \tag{7}$$

where $\delta n_{\omega i}$ and $\delta B_{\|\omega i}$ are determined from an FFT of the data in the ith data segment. At each discrete frequency, $R_{\|n_p}$ is the cosine of the phase angle of Q, and we define the coherence C of this phase angle to be equal to the magnitude of Q. (Alternate definitions of Q do exist; see, for example, Papoulis [1965] and the
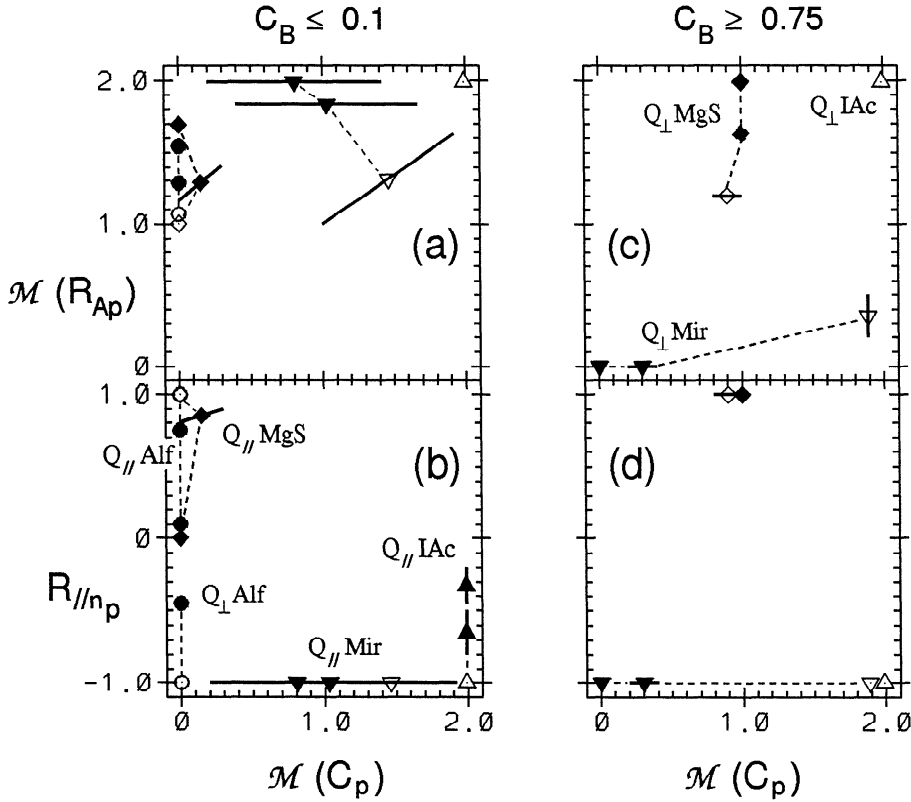
Figure 2. (a) $\mathcal{M}(R_{Ap})$ and (b) $R_{\|n_p}$ versus $\mathcal{M}(C_p)$ for $C_B \leq 0.1$. The theoretical values for each mode are plotted for $\beta_{\|p} = 0.10$, $\beta_{\|p} = 1.0$, and $\beta_{\|p} = 10.0$ with the open symbol indicating the low $\beta_{\|p} = 0.10$ value. (c) Same as Figure 2a and (d) same as Figure 2b, except for $C_B \geq 0.75$. The solid lines show the variation of the theoretical values with respect to the allowed range of θ_{kB} (5–20° for a quasi-parallel mode or 65–85° for a quasi-perpendicular mode), while the dashed lines connect for each mode the points corresponding to different values of $\beta_{\|p}$. The open symbol at the top left corner of Figure 2b is a superimposed open circle and diamond. The abbreviations are defined in the text.

appendix.) The frequency resolution for $R_{\|n_p}$ will be decreased relative to that of the original data by a factor equal to N_C. We choose the value of N_C for each event so that eight discrete frequencies are resolved in the frequency range being analyzed. (The frequency ranges vary for each event; they are listed in Table 2b. The values of N_C are listed in Table 2c.) We calculate an average value and standard deviation for $R_{\|n_p}$ using the values corresponding to these eight frequencies.

Note that if all the data segments have the same phase angle, the phase angle coherence C will be unity. For a large number of random angles, C should be close to zero. We, in general, assume that $R_{\|n_p}$ is meaningful only if C is greater than 0.5. (If half of the wave power is a pure coherent oscillation and half of the wave power is random, a large number of equal length vectors should give $C = 0.5$.) Of course, if N_C is small, C itself may be significantly in error and it must be interpreted with care. We discuss this more in the context of the specific events (section 3.2).

2.5. Mode Deviation D(mode)

We combine all of the transport ratios simultaneously to parameterize the difference between the observed fluctuation properties and the theoretical predictions for each mode. First, we define our ratios such that each has a total variation of 2. To do this, we begin by mapping the values of R_{Ap} and C_p to a variation range of 2 using the ratio mapping $\mathcal{M}()$ described in (6). We multiply the values of C_B by 2, so they also vary over the range 0 to 2. The value of $R_{\|n_p}$ already has a variation range of 2, from –1 to +1. For a given mode m and transport ratio t, we define the deviation D_{mt} as the absolute value of the difference between the observed transport ratio and the mode theoretical value. In general, the observed values may be represented by a range of values owing to the experimental uncertainty in measured quantities. In such a case we let D_{mt} be zero if the range overlaps the mode theoretical value. If the ranges do not overlap, D_{mt} is equal to the smallest dif-

ference between the theoretical value and any value in the observational range. Finally, for each mode, we define the total deviation $D(m)$ as the root-mean-square value of the transport ratio deviations D_{mt}; that is,

$$D(m) = \left(\frac{1}{N_T} \sum_t D_{mt}^2 \right)^{1/2}, \qquad (8)$$

where m represents one of the eight modes of Table 1 and N_T is the number of transport ratios used (four, if $R_{\|n_p}$ is used, three otherwise). The mode deviation $D(m)$ is a measure of how well the observations agree with a particular theoretical mode.

The theoretical values vary over the angular range of θ_{kB}, but they do not vary independently of each other. Consider, for instance, the variation in R_{Ap} and C_p for the quasi-parallel mirror mode in Table 1 or Figure 2a. The smallest value of R_{Ap} occurs when C_p also has its smallest value (from Table 1, it can be seen that this occurs at the smallest $\theta_{kB} = 5°$). Denton et al. [1995] took account of the theoretical variation as if these values were independent. They calculated the smallest value for each D_{mt}, allowing the theoretical value to vary over its entire range. Our present method is somewhat different. Consider the two angular limits for a particular mode. At these two limits there are four values corresponding to our transport ratios (or ratio-mapped values). These two sets of numbers define two points in four-dimensional transport ratio space. Consider the line joining these two points and a finite set of points evenly spaced along this line, with the first point at one end of the line corresponding to one angular limit and the last point at the other end corresponding to the other angular limit. We used 11 points in all, so that we have 11 sets of theoretical transport ratios for any mode. For each mode, we calculated a tentative value for the mode deviation $D(m)$ using each of these points and then kept the smallest value for the actual mode deviation. The net effect is that the error bars for each theoretical mode lead to an error line in four-dimensional transport ratio space rather than a four-dimensional error box. The difference is especially significant for the quasi-parallel mirror mode which has large variation in $R_{\|n_p}$ and C_p.

If the mode deviation $D(m)$ is 0, then the mode theoretical transport ratios are in total agreement with the observed ratios to within experimental uncertainty. If the mode deviation is 2, the observed mode has exactly the opposite properties of the theoretical mode (if the observed R_{Ap} is 0, the mode R_{Ap} must be infinity; and if the observed $R_{\|n_p}$ is -1, the theoretical value must be +1). A mode deviation of order unity represents no significant agreement between the observed and theoretical values. Thus we consider the observed mode to be in good agreement with the theoretical mode if $D(m)$ is significantly less than unity.

If more than one theoretical mode has a small value of $D(m)$, then both theoretical modes agree with the observations. In order to have a measure of how unique our identification is, we calculate $[D(\text{best}) - D(\text{2nd})]/D(\text{best})$, where $D(\text{best})$ and $D(\text{2nd})$ are the mode deviations of the best fitting (smallest value of $D(m)$) and second best fitting modes. A large value of this quantity indicates that our identification is unique [$D(\text{2nd})$ is significantly larger than $D(\text{best})$]. Roughly, a value of $[D(\text{best}) - D(\text{2nd})]/D(\text{best})$ greater than unity indicates a unique identification. On the other hand, we should keep in mind that if $D(\text{best})$ and $D(\text{2nd})$ are both very small (much less than unity), they are both in essential agreement with the observations, regardless of the value of $[D(\text{best}) - D(\text{2nd})]/D(\text{best})$.

The purpose of the mode deviation is to give us an objective measure of how well observed transport ratios agree with theoretical values. Without such an objective measure, it is not clear how good agreement is nor whether the agreement with one mode is any better than with another. Certainly, other types of quantities could be defined, such as the maximum amount that any one observed transport ratio value differs from those of a theoretical mode, but we believe that some such measure must be defined in order to make an objective comparison.

3. Data

3.1. General Description of IRM Data

The ion density and velocity corresponding to the energy range 20 eV–40 keV are measured by the IRM spacecraft roughly every spin period, which is approximately 4.3 s [Paschmann et al., 1985]. Since IRM has no ion composition information at these energies, we assume the ion distibution function consists entirely of protons (see Paschmann et al. [1986] for a discussion of the error involved). From the time series of these plasma moments we calculate the Fourier transforms necessary to calculate the transport ratios. We linearly detrend the data and apply a Welsh window before Fourier transforming. The highest possible frequency for calculating transport ratios based on the plasma fluctuations is the Nyquist frequency, which is approximately 0.1 Hz.

The magnetic field data are sampled at a much higher rate, every 31 or 62 ms depending on the mode of operation [Lühr et al., 1985]. Spin averages of the magnetic field data were used in computing the transport coefficients, since these matched the time resolution of the plasma data. However, the full-resolution magnetic field data were used as a check to see that the spin-averaged magnetic data were reliable. We have confined our study to frequencies below 0.04 Hz, and for these frequencies the low-resolution data are in quali-

Table 2a. Event Data: Times

Event	Region of the Magnetosheath	Date	Start Time, UT	End Time, UT
1	middle	Sept. 1, 1984	0816:02	0908:02
2	middle	Nov. 12, 1984	0730:04	0801:38
3	middle	Oct. 24, 1985	1104:00	1203:58
4	outer	Sept. 1, 1984	0932:20	1010:01
5	outer	Nov. 12, 1984	1020:04	1040:02
6	outer	Nov. 1, 1985	0853:20	0932:52
7	inner	Oct. 8, 1985	0900:00	0911:06
8	inner	Sept. 17, 1984	2200:06	2210:55

tative agreement with the high-resolution data for all cases studied here.

3.2. General Description of the Events

We examined the IRM data for eight events. The dates and times of these events are given in Table 2a. Out of these, events 1–3 are from the middle magnetosheath, events 4–6 are from the outer magnetosheath, and events 7 and 8 are from the inner magnetosheath. "Middle," "outer," and "inner" here are determined by temporal position within a period of magnetosheath data. By inference, they are assumed to correspond to rough spatial position, with the inner magnetosheath corresponding to a location near the magnetopause and the outer magnetosheath corresponding to a location near the bowshock. (Events with discontinuous or rapid changes in the equilibrium parameters were avoided.) Events 7 and 8 in Table 2a were included in the study of *Denton et al.* [1995], where they were events 3 and 17, respectively. That study concentrated totally on the inner magnetosheath. Though most inner magnetosheath waves were identified as the quasi-perpendicular mirror mode, events 7 and 8 here were identified as the quasi-parallel mirror mode. Since we have made some changes in our method that would make this identification less likely, we are reexamining them here. No aspect of our new method has made identification of the quasi-perpendicular mirror mode less likely, so the identification of these waves in the inner magnetosheath (close to the magnetopause) is unchanged.

Table 2b gives for each event the event number, region, L shell, local time (LT) (GSE coordinates), duration in minutes, frequency range used in this study, proton gyrofrequency F_{cp}, and frequency range normalized to the proton gyrofrequency F/F_{cp}. We evaluate the transport ratios over the frequency range given in Table 2b. We use the average value over the frequency range for C_B and $R_{\parallel n_p}$ and the log average value for R_{Ap} and C_p. The values of C_B, $R_{\parallel n_p}$, and R_{Ap} are averaged using a weighting proportional to the total magnetic power at that frequency. The value of $R_{\parallel n_p}$ is found from a similar average as described in section 2.4.

For each event we have chosen a single frequency range. We examined only frequencies that corresponded to at least 16 wave periods during the observation time. (Event 3 was an exception, with only 12 wave periods at the lowest frequency.) We have also limited the maximum frequency to 0.04 Hz in order to avoid complications in the Fourier analysis at higher frequencies due to the fact that in the most common mode, the plasma data were not sampled evenly [*Paschmann et al.*, 1985]. In all but one case the dominant waves were below 0.04 Hz. (In that one case, September 1, 1984, event 1, the waves above 0.04 Hz appear to have transport ratios similar to those below 0.04 Hz.) In most cases a single frequency range was sufficient to characterize the dominant waves. In cases where different frequency ranges might be considered, only one frequency range was selected for analysis in this study. In all cases, the fre-

Table 2b. Event Data: General Information

Event	Region of the Magnetosheath	L	LT, GSE	Duration, min	Frequency, Hz	F_{cp}, Hz	F/F_{cp}
1	middle	12	1230	52	[0.01, 0.04]	0.43	[0.023, 0.091]
2	middle	12.5	0800	32	[0.025, 0.04]	0.51	[0.049, 0.078]
3	middle	12	1330	60	[0.005, 0.012]	0.35	[0.014, 0.034]
4	outer	13	1230	38	[0.01, 0.04]	0.30	[0.033, 0.133]
5	outer	15	0830	20	[0.015, 0.04]	0.26	[0.058, 0.15]
6	outer	11	1000	39	[0.005, 0.025]	0.41	[0.012, 0.061]
7	inner	10.5	1130	11	[0.01, 0.04]	0.88	[0.011, 0.045]
8	inner	11	1130	11	[0.023, 0.04]	0.21	[0.11, 0.19]

F_{cp} is the proton gyrofrequency; F/F_{cp} is frequency normalized to F_{cp}. Brackets enclose the lower and upper limits of the frequency range analyzed.

Table 2c. Event Data: Transport Ratios

Event	$\beta_{\|p}$	$\left(\frac{T_\perp}{T_\|}\right)_p$	$\frac{|\delta B^2|}{B_0^2}$	C_B	R_{Ap}	C_p	$R_{\|n_p}$	C	N_C
1	3.0	1.4	0.011	0.66 ± 0.11	0.37 ×/ 1.3	0.043 ×/ 1.2	-0.98 ± 0.02	0.73	23
2	1.1	1.6	0.0026	0.67 ± 0.06	0.33 ×/ 1.2	0.24 ×/ 1.3	-0.90 ± 0.17	0.76	7
3	5.4	1.4	0.032	0.22 ± 0.07	0.14 ×/ 1.2	0.0059 ×/ 1.4	-0.07 ± 0.61	0.44	6
4	6.6	1.3	0.043	0.18 ± 0.09	0.54 ×/ 1.3	0.024 ×/ 1.9	-0.01 ± 0.78	0.40	16
5	10.0	0.97	0.24	0.08 ± 0.02	0.61 ×/ 1.2	0.035 ×/ 1.4	0.09 ± 0.76	0.40	7
6	7.3	1.3	0.0088	0.23 ± 0.08	0.40 ×/ 1.7	0.036 ×/ 2.0	0.01 ± 0.76	0.44	11
7	0.21	1.1	0.0017	0.15 ± 0.06	0.59 ×/ 1.3	3.3 ×/ 1.4	-0.94 ± 0.04	0.96	4
8	25.	0.95	0.094	0.30 ± 0.10	0.24 ×/ 1.2	0.0071 ×/ 1.9	-0.17 ± 0.45	0.00	2

The notation "×/" indicates a multiplicative error factor determined from the standard deviation of the log value. Variables not defined in Table 1 are C, the phase angle coherence, and N_C, the number of independent data segments from which coherence was measured.

quency range is well below the He^{2+} gyrofrequency at 0.5 F_{cp}.

The values of $\beta_{\|p}$, proton temperature ratio $(T_\perp/T_\|)_p$, ratio of wave to background magnetic energy $|\delta B|^2/B_0^2$, and values of the transport ratios C_B, R_{Ap}, C_p, and $R_{\|n_p}$ are listed for each event in Table 2c. The errors for R_{Ap} and C_p are multiplicative, as they are found from the standard deviation of the log value. Also listed in Table 2c are the phase angle coherence of density and parallel magnetic fluctuations C and the number of independent data segments from which that coherence was measured N_C.

A high value of the phase angle coherence C indicates that $R_{\|n_p}$ is meaningful, at least if N_C is large enough that the error in measurement of C is low. Normally, a large value for C coincides with a well-defined value of $R_{\|n_p}$. For instance, event 1 has a well-defined value $R_{\|n_p} = -0.98 \pm 0.02$ and a large phase angle coherence $C = 0.73$. On the other hand, event 4 has $R_{\|n_p} = -0.01 \pm 0.78$; in this case the uncertainty covers most of the allowable range of $R_{\|n_p}$. The value of $C = 0.40$ is, in this case, low. (None of our events has a well-defined $R_{\|n_p}$ with low phase angle coherence; this might result if there is an underlying nondominant mode with well defined $R_{\|n_p}$, while the dominant mode, or noise, has poorly defined $R_{\|n_p}$. A simpler procedure for determining the relevance of $R_{\|n_p}$ would be to use the Fourier analysis of the entire data segment and ignor $R_{\|n_p}$ if the standard deviation is large.)

We estimate the error in our phase angle coherence as $1/\sqrt{N_C}$. Clearly, for event 8, with $N_C = 2$, the phase angle coherence is meaningless. For values of $N_C < 10$, we regard the phase angle coherence as having doubtful validity. A low number of data segments N_C is likely to lead to a large phase angle coherence. In those cases with $C > 0.5$ and $N_C < 10$ (which number three out of the eight events), we have examined the values of $R_{\|n_p}$ with respect to frequency in order to get an idea of whether or not the value of $R_{\|n_p}$ is meaningful. Basically, we look for consistency of $R_{\|n_p}$ across varying frequency. This method is almost equivalent to check-

ing that the uncertainty in $R_{\|n_p}$ in Table 2c is small (in an automated scheme, one could do just this); but we can also check the frequency variation of $R_{\|n_p}$ across frequencies not included in the range we picked for analysis. In every case, except one, we decided that $R_{\|n_p}$ was meaningful when C was greater than 0.5. For event 8, the phase angle coherence was large (not surprisingly since N_C was only 2), but $R_{\|n_p}$ seemed to vary randomly with respect to frequency. Therefore we decided that $R_{\|n_p}$ was meaningless for this event, which we indicate by listing 0.00 for the phase angle coherence in Table 2c. In summary, we consider $R_{\|n_p}$ to be a meaningful quantity only for those events for which the listed value of C in Table 2c is greater than 0.5.

In Figure 1a, we plot power spectra $|\delta B|^2/\Delta f$ (nT^2/Hz) of the magnetic fluctuations parallel (solid curve) and perpendicular (dashed curve) to $\mathbf{B}_0$ versus frequency in hertz for the November 12, 1984, event (event 5 in Table 2b). This event was in the outer magnetosheath. In Figures 1b–1d, we plot the transport ratios C_B, R_{Ap}, and C_p, respectively. The phase difference between density and parallel magnetic fluctuations $\phi_{\delta n} - \phi_{\delta B_{//}}$ is plotted in Figure 1e. The value of $R_{\|n_p}$ is found from the cosine of this angle. Note then that values of $\phi_{\delta n} - \phi_{\delta B_{//}} = 0°$ correspond to $R_{\|n_p} = 1$ while values of $\phi_{\delta n} - \phi_{\delta B_{//}} = 180$ or $-180°$ correspond to $R_{\|n_p} = -1$. We plotted $\phi_{\delta n} - \phi_{\delta B_{//}}$ rather than $R_{\|n_p}$ in order to see if there was ever a consistent preference for $\phi_{\delta n} - \phi_{\delta B_{//}} = 90$ versus $-90°$, a difference that would not be perceived by looking at $R_{\|n_p}$. (We have not clearly seen such a preference in any of the events we have examined. It is certainly absent in Figure 1e, for which positive and negative values of $\phi_{\delta n} - \phi_{\delta B_{//}}$ seem to be equally likely.) The phase coherence C is shown in Figure 1f. Our chosen frequency range for analysis was 0.015–0.04 Hz (Table 2b). Figure 1a shows that there is a peak in transverse magnetic fluctuations within this frequency range.

Figure 1e shows that $\phi_{\delta n} - \phi_{\delta B_{//}}$ varies considerably over the frequency range, leading to $R_{\|n_p} = 0.09 \pm 0.76$ (Table 2c). The phase angle coherence C is low = 0.40,

Table 2d. Event Data: Mode Deviations

Event	C_B	C				Deviations				
			$Q-\parallel$ MgS	$Q-\perp$ MgS	$Q-\parallel$ Alf	$Q-\perp$ Alf	$Q-\parallel$ IAc	$Q-\perp$ IAc	$Q-\parallel$ Mir	$Q-\perp$ Mir
1	0.66	0.73	0.87	0.87	0.87	0.73	0.87	0.87	0.87	0.14
2	0.67	0.76	0.87	0.87	0.87	0.76	0.87	0.87	0.87	0.14
3	0.22	0.48	0.81	1.00	0.76	0.77	1.00	1.00	1.00	0.53
4	0.18	0.30	0.53	1.00	0.47	0.49	1.00	1.00	0.75	0.62
5	0.08	0.41	0.54	1.00	0.47	0.50	1.00	1.00	0.75	0.80
6	0.23	0.33	0.53	1.00	0.49	0.51	1.00	1.00	0.76	0.53
7	0.18	0.76	0.87	0.87	0.87	0.81	0.62	0.82	0.38	0.56
8	0.30	0.00	0.79	1.00	0.75	0.78	1.00	1.00	1.00	0.42

Key to modes is as follows: $Q-\parallel$ corresponds to $5° < \theta_{kB} \lesssim 20°$; $Q-\perp$, $60° \lesssim \theta_{kB} < 85°$; MgS, magnetosonic; Alf, Alfvén; IAc, ion acoustic; and Mir, mirror.

and on the basis of this, we do not use $R_{\parallel n_p}$ for the identification of the waves for this event.

4. Results

4.1. Middle Magnetosheath Events

Now we turn to a specific discussion of the events in particular regions. We begin with events 1–3 in the middle magnetosheath (Table 2b). For events 1 and 2, the phase angle coherence C is greater than 0.5, but event 3 had $C = 0.44 < 0.5$ (Table 2c). We use $R_{\parallel n_p}$ as one of our transport ratios for events 1 and 2 but not for event 3.

Table 2d lists for each event the mode deviation between the observations and the theoretical modes; C_B and C are also given. There is never a great difference between the mode deviations for the $Q-\parallel$ magnetosonic and $Q-\parallel$ Alfvén modes; these are essentially the same mode as discussed in section 2.3 (see Figure 2). Data in Table 2d for events 1–3 show that in each case the mode deviation is smallest for the $Q-\perp$ mirror mode. This is especially true for events 1 and 2; for these events, the mode deviation for the $Q-\perp$ mirror mode (0.14 for both events) is more than 5 times smaller than those of the other theoretical modes. For event 3, the mode devia-

tion for the $Q-\perp$ mirror is 0.53, indicating not nearly as good a match. (Recall that the mode deviation should be significantly less than unity for a good fit to theory.) The value of $D(m)$ for the next best fitting mode is 0.76 ($Q-\parallel$ Alfvén mode). While $[D(\text{best})-D(\text{2nd})]/D(\text{best})$ is significantly greater than unity for events 1 and 2, indicating that these events are well identified, it is less than unity for event 3. The best identification for event 3 is the quasi-perpendicular mirror mode, but identification in terms of the $Q-\parallel$ Alfvén mode cannot be ruled out.

To see why these events were best described by the $Q-\perp$ mirror mode, one can compare the observed transport ratios in Table 2c to the theoretical transport ratios in Table 1. However, it is easier to see the comparison presented pictorially. In Figure 3, we present the theoretical mode transport ratios in a format similar to that of Figure 2. There are a few differences. First, we chose to plot the theoretical values as open symbols for plasma $\beta_{\parallel p} = 3.0$ only; this value is fairly typical for events 1–3 which have values of $\beta_{\parallel p}$ ranging from 1.1 to 5.4. The error lines for the theoretical values are now dashed. Only the best fitting theoretical modes, the $Q-\perp$ mirror mode and the Alfvén modes, have labels indicating their values. Values of transport ratios for events 1–3 are indicated by rectangles, which indi-

Table 2e. Event Data: Best Fitting Modes

Event	C_B	C	Best Fitting Mode	$D(\text{Best})$	Second Best Mode	$D(\text{2nd})$	$\dfrac{D(\text{2nd}) - D(\text{Best})}{D(\text{Best})}$
1	0.66	0.73	$Q-\perp$ Mir	0.14	$Q-\perp$ Alf	0.73	4.21
2	0.67	0.76	$Q-\perp$ Mir	0.14	$Q-\perp$ Alf	0.76	4.43
3	0.22	0.48	$Q-\perp$ Mir	0.53	Alf/$Q-\parallel$ MgS	0.76	0.43
4	0.18	0.30	Alf/$Q-\parallel$ MgS	0.47	$Q-\perp$ Mir	0.62	0.32
5	0.08	0.41	Alf/$Q-\parallel$ MgS	0.47	Mir	0.75	0.60
6	0.23	0.33	Alf/$Q-\parallel$ MgS	0.49	$Q-\perp$ Mir	0.53	0.08
7	0.18	0.76	$Q-\parallel$ Mir	0.38	$Q-\perp$ Mir	0.56	0.47
8	0.30	0.00	$Q-\perp$ Mir	0.42	Alf/$Q-\parallel$ MgS	0.75	0.79

$Q-\parallel$ corresponds to $5° < \theta_{kB} \lesssim 20°$; $Q-\perp$, $60° \lesssim \theta_{kB} < 85°$; MgS, magnetosonic; Alf, Alfvén; IAc, ion acoustic; and Mir, mirror.
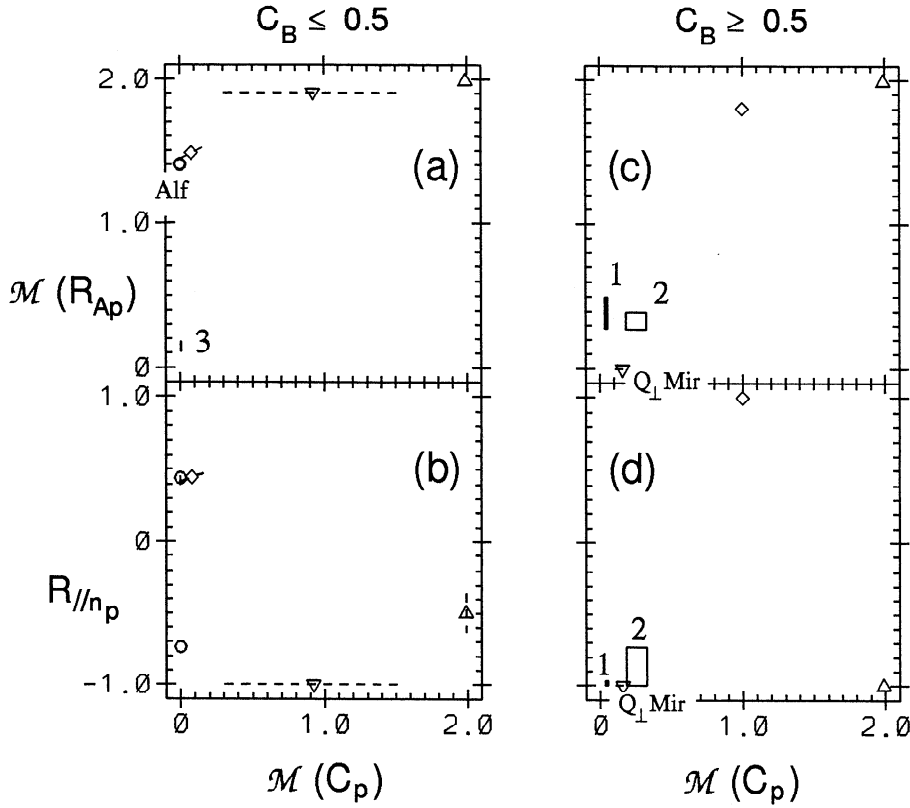
Figure 3. Same as Figure 2, except with rectangles showing the extent of the error bars for each of the middle magnetosheath events 1–3. Open symbols indicate the theoretical mode values for $\beta_{\|p} = 3.0$, a typical value for these events. The lines showing the theoretical mode variation with respect to θ_{kB} are now dashed.

cate the extent of the error bars given in Table 2c. With our present method, the observed mode is considered to have transport ratios consistent with any value within the box. Note the numerical labels for the events in Figures 3a, 3c, and 3d. We have plotted rectangles in Figures 3c and 3d for events 1 and 2, since these have $C_B > 0.5$. Error boxes for event 3 are plotted in Figure 3a, since it has $C_B < 0.5$. We do not plot the error box in Figure 3b, since we ignore $R_{\|n_p}$ owing to the low value of C. Thus only Figure 3a and possibly Figure 3c are relevant to the identification of event 3.

Note that the rectangular error boxes for events 1 and 2 are very close to the theoretical values for the $Q-\perp$ mirror mode; it is clear that these events are best described by that mode. From the location where the error box for event 3 is plotted in Figure 3a, it appears at first that event 3 ought to be identified as a quasi-parallel mode (or the $Q-\perp$ Alfvén mode). However, if we were to transfer the error box for event 3 over to Figure 3c, we would find the agreement with the $Q-\perp$ mirror mode to be excellent. We see then that event 3 has excellent agreement with the $Q-\perp$ mirror mode for R_{Ap} and C_p but not for C_B. This difference in C_B is less than the difference in $\mathcal{M}(R_{Ap})$ for the Alfvén mode (Figure 3a). Thus the mode turns out to be best identified as the $Q-\perp$ mirror mode. Possibly,

this mode is a mirror mode at an angle less than $60°$. On the other hand, Alfvén wave identification cannot be ruled out. (We note that a plot for event 3 similar to Figure 1 shows that observed waves have even smaller Alfvén ratio R_{Ap} at lower frequencies where the wave power is greater. It is the value of R_{Ap} that makes an Alfvén wave identification difficult.

Our mode deviation information is summarized in Table 2e. First, we again list C_B and C. These values are important for our interpretation of the figures. The value of C_B tells us to what extent we should consider it important that an event is plotted in the $C_B < 0.5$ or $C_B > 0.5$ section of a figure. The phase coherence C tells us whether or not $R_{\|n_p}$ is meaningful. In Table 2e we list the best fitting mode (which in the case of events 1–3 is the $Q-\perp$ mirror mode) and the mode deviation of this best fitting mode D(best). We then list the second best fitting mode and its mode deviation. In the case of event 3, we list Alf/$Q-\|$ MgS for the second best fitting mode; this means either the $Q-\|$ or $Q-\perp$ Alfvén mode or the $Q-\|$ magnetosonic mode. When $R_{\|n_p}$ is not known, these modes are almost equivalent, as can be seen from Figure 2a and from the similar values for $D(m)$ in Table 2d. The final column of Table 2e lists $[D(\text{best}) - D(\text{2nd})]/D(\text{best})$. While the values are high for events 1 and 2, it is only 0.43 for event 3. From
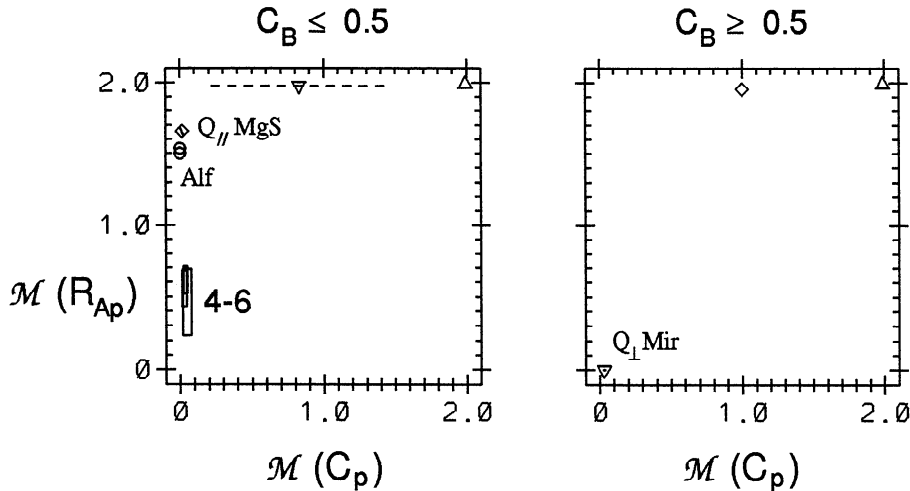
Figure 4. Same as Figure 3a and 3c, except for outer magnetosheath events 4–6 with theoretical mode values for a typical value $\beta_{\|p} = 8$.

these values, we would say that events 1 and 2 are well identified as the quasi-perpendicular mirror mode. The best identification for event 3 is the quasi-perpendicular mirror mode, but an Alfvén wave identification cannot be ruled out.

4.2. Outer Magnetosheath Events

Now we consider the outer magnetosheath events 4–6. In this case, the phase coherence $\mathcal{C}$ between δn_p and $\delta B_\|$ was small for each of the events, so we did not make use of $R_{\|n_p}$. Examination of Tables 2d and 2e shows that events 4 and 5 are best identified as Alfvén-like modes (Alfvén or $Q-\|$ magnetosonic modes). On the basis of the values in Table 2d, identification as the mirror mode cannot be ruled out. However, event 5 had a value of cross helicity σ_{cp} (equation (5)) equal to -0.64 ±0.07. The magnitude of this value is large enough to rule out the mirror mode so that event 5 is well identified. (No other event had $|\sigma_{cp}|$ larger than 0.41.) Event 6 is equally well identified as an Alfvén-like mode or the $Q-\perp$ mirror mode. Alfvén waves have been identified in this region previously (see, for instance, *Hubert* [1994]).

Figure 4 shows events 4–6 plotted with a format similar to that of Figure 3. Only Figures 4a and 4c are displayed, since the value of $R_{\|n_p}$ is not considered relevant. In this case, the error boxes for all three events overlap. It appears from the event boxes that the best fitting modes are the Alfvén or $Q-\perp$ mirror modes.

Anderson et al. [1994] found for regions in the magnetosheath closer to the magnetopause that mirror modes were observed under conditions of high beta ($\beta_{\|p} \gg 1$), while ion cyclotron (Alfvén) waves were observed when beta was low ($\beta_{\|p} \ll 1$). This was attributed to properties of the mirror and proton cyclotron instabilities, both of which are driven by temperature anisotropy ($T_{\perp p}/T_{\|p} > 1$). The fact that we observe Alfvén waves in the outer magnetosheath for $\beta_{\|p} \gg 1$ and modest

$T_{\perp p}/T_{\|p}$ (see Table 2c) suggests that the observed waves are either not produced by an anisotropy-driven instability or they were produced in the more anisotropic environment just downstream of the bow shock.

4.3. Inner Magnetosheath Events With Small C_B

Denton et al. [1995] examined 17 events that were temporally close to the magnetopause. Out of these, 11 events had dominant parallel magnetic fluctuations ($C_B > 0.5$), and of these 11, 9 were well identified as the the $Q-\perp$ mirror mode. None of the changes to our method makes an identification of the $Q-\perp$ mirror mode less likely, so this result stands. On the other hand, they also showed that 2 of the 17 events were well identified as the $Q-\|$ mirror mode. There are several changes we have made that make this identification less likely. First, there was an error in the work by *Denton et al.* [1995] such that C_p for the $Q-\|$ mirror mode had a broader range of values than it should have had. Our limitation of the angular range of quasi-parallel modes to 0–20° (section 2.1) further limits the range of values of several $Q-\|$ mirror mode transport ratios. Finally, using an error line rather than a four-dimensional error box (section 2.5) decreases the space over which a theoretical mode can fit the observations. Use of the error line will have its greatest effect for a mode with large error bars in individual transport ratios and will therefore have its greatest effect on the $Q-\|$ mirror mode (Table 1 or Figure 2 shows that the error ranges for the $Q-\|$ mirror mode are the greatest). (We also made some changes in the way we calculate $R_{\|n_p}$ (section 2.4), but this could have the effect of making an identification in terms of the $Q-\|$ mirror mode more or less likely.)

Taking into account these changes in method, it is appropriate for us to examine again those events that were well identified as the $Q-\|$ mirror mode in the ear-
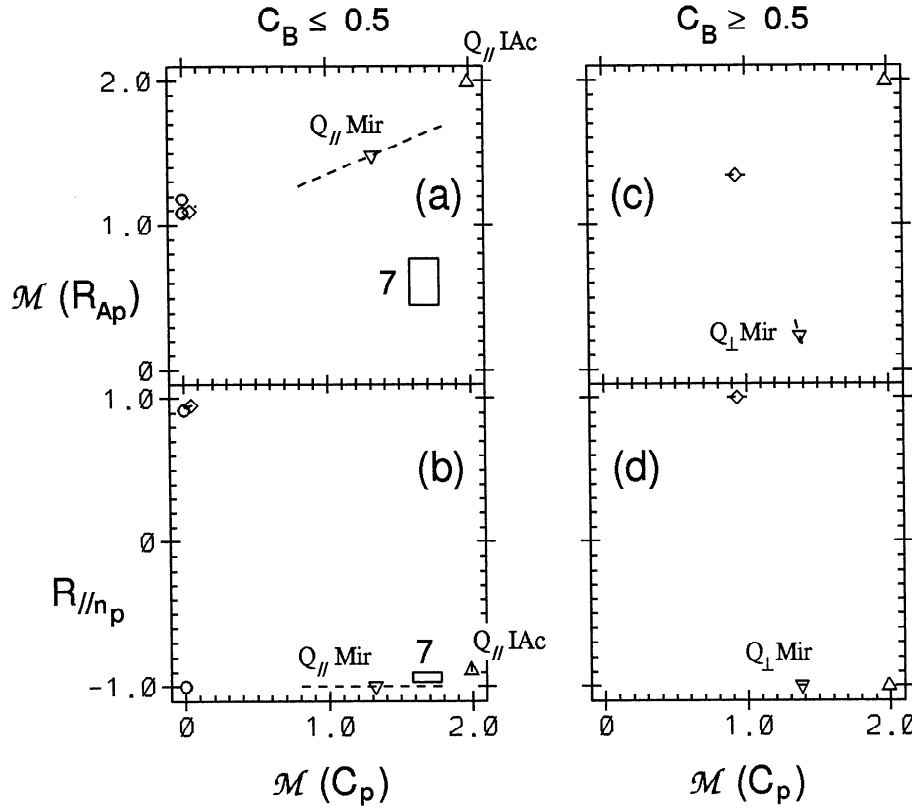
Figure 5. Same as Figure 3, except for inner magnetosheath event 7 with theoretical mode values for $\beta_{\|p} = 0.21$, the beta value for this event.

lier study. These events, 7 and 8 in Table 2, correspond to events 3 and 17, respectively, in Table 4 of *Denton et al.* [1995]. Both events 7 and 8 had a small period of observation and a correspondingly small number of data segments for calculation of $R_{\|n_p}$ ($N_C = 4$ and 2, respectively). Therefore we could not depend on C to give us an idea of whether or not $R_{\|n_p}$ was reliable. From the low variation of $R_{\|n_p}$ over the frequency range (see the $R_{\|n_p}$ column of Table 2c), we decided to use the value of $R_{\|n_p}$ for the identification of event 7 but not for the identification of event 8. (The results in the appendix support our use of $R_{\|n_p}$ for event 7.) We have indicated this by making the value of C zero for event 8 in Table 2c (see section 3.2). (Owing to the low values of N_C, both measured values of C are close to unity; for the case of event 7 this high value of C remains in Table 2c because we decided to accept its value of $R_{\|n_p}$.)

Because of the vastly different values of $\beta_{\|p}$ for events 7 and 8 (0.21 and 25, respectively), we have plotted them separately in Figures 5 and 6. (The different plots are needed because of the different theoretical mode transport ratio values.) From Figures 5a and 5b, the transport ratios for event 7 appear to be closest to those corresponding to the $Q-\|$ mirror mode. On the other hand, looking at Figures 5c and 5d, we see that aside from the value of $C_B = 0.15$, which caused us to put the error boxes for event 7 in Figures 5a and 5b rather than in Figures 5c and 5d, the transport ratios of event 7 match those of the $Q-\perp$ mirror mode. Table 2e shows

that event 7 is best identified as the $Q-\|$ mirror mode but that the match to the $Q-\perp$ mirror mode is not much worse. An identification in terms of the $Q-\|$ ion acoustic mode cannot be ruled out.

Because the linear $Q-\|$ mirror mode is heavily damped [*Denton et al.*, 1995] and this mode has not ever been identified by independent means, we examined some aspects of the wave polarization more closely in the appendix. The results are inconclusive; the observed wave polarization is not inconsistent with that of the $Q-\|$ mirror mode, but it does not prove that the waves are without doubt the $Q-\|$ mirror mode.

Aside from the value of C_B, the transport ratios of event 8 match well with the $Q-\perp$ mirror mode (Figure 6). Event 8 is best identified as the $Q-\perp$ mirror mode, but identification as an Alfvén-like mode cannot be ruled out (Table 2e). Thus neither event 7 or 8 is well identified using our current method.

5. Discussion

Our method gives us a measure of how well each theoretical mode fits the observed waves [$D(m)$]. In this study, the best fitting mode was the quasi-perpendicular mirror mode for the middle magnetosheath events and an Alfvén-like (Alfvén or quasi-parallel magnetosonic) mode in the outer magnetosheath. In the inner magnetosheath, the best fitting mode was the quasi-perpendicular mirror mode for event 8 (and
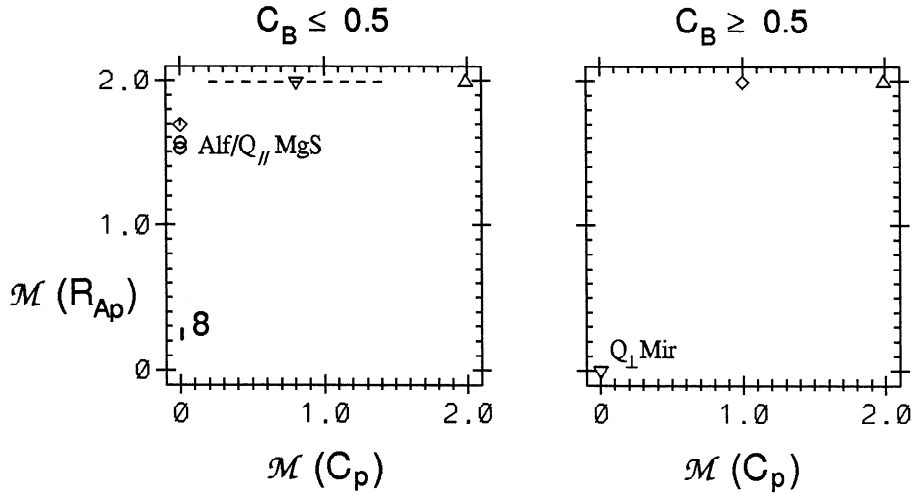
Figure 6. Same as Figure 3a and 3c, except for inner magnetosheath event 8 with theoretical mode values for $\beta_{\|p} = 25$, the beta value for this event.

most of the events of *Denton et al.* [1995]) and the quasi-parallel mirror mode for event 7. Our identifications agree with those of *Song et al.* [1994] in the middle and outer magnetosheath. In the inner magnetosheath, we find the mirror mode, whereas they claimed to identify the ion acoustic ("slow") mode. That identification was based on the fact that the observed wave had a finite phase frequency.

If we take $[D(\text{best}) - D(\text{2nd})]/D(\text{best}) > 1$ as a condition for a well-identified (that is, uniquely identified) mode, most of the events in this study were not well identified. From Table 2e, we see that only events 1 and 2 had $[D(\text{best}) - D(\text{2nd})]/D(\text{best}) > 1$. This means that for the other events, we cannot rule out the possibility that the observed wave could be other than the best fitting mode. Our method certainly narrows down the possible identifications. For instance, from Table 2d we see that it is very unlikely that the observed waves for any of the events are the quasi-perpdendicular magnetosonic mode; but, ideally, we would like to have a unique identification for each event.

Unique identification may be easier for modes with dominant parallel magnetic fluctuations, since these modes are better separated in transport ratio space than the modes with dominant perpendicular fluctuations (compare Figures 2c and 2d to Figures 2a and 2b). Part of the problem for finding a unique identification is that the parallel phase ratio $R_{\|n_p}$ is not always well defined. This often occurs when the density and parallel magnetic fluctuations are small.

It is apparent that more information would assist the mode identification process. One question that comes to mind is whether there exist additional transport ratios that would give additional information. One possibly useful quantity is the ratio of parallel to total velocity fluctuations (we might call this C_v in analogy to C_B). In addition to $R_{\|n_p}$, one can imagine several other phase angles involving fluctuations of the den-

sity, velocity, and magnetic field. Perhaps these could be complementary; that is, one might be well defined when another is not. There might be useful information in the transport ratios calculated using heavy ions or electrons. The difficulties with mode identification demonstrated here point out the value of multispacecraft or multiantenna studies. With multiple spacecraft and/or multiple antennas, it is possible to determine **k** and the polarization in the plasma frame (left versus right handed; see, for instance, *Le et al.* [1992, and references therein]).

There are a number of complications that may lead to difficulty in mode identification. Inhomogeneity may significantly affect the modes. As mentioned above, *Song et al.* [1994] identified the slow mode (our ion acoustic mode) in the inner magnetosheath based on the fact that the observed wave had a finite phase velocity. Results by *Omidi and Winske* [1995] and *Johnson and Cheng* [1997] suggest that the mirror mode may pile up at the magnetopause, thus obtaining a finite phase velocity. While our method does not seem to be imperiled in this case, there may be other effects of inhomogeneity that do significantly affect our results. Simulations including the effect of inhomogeneity would be helpful. *Lacombe et al.* [1995] show evidence for mode coupling (invoked to explain the detailed properties of their He^{2+} cut-off mode). This could also possibly be due to inhomogeneity or possibly nonlinear effects. Non-Maxwellian features in the distribution function could affect the transport ratios. See *Schwartz et al.* [1996] for a discussion of possible complications. Perhaps the greatest difficulty involves the superposition of different modes. Such a superposition will naturally lead to transport values that are intermediate in value. Noise could have a similar effect. Examination of Figure 2a reveals that the quasi-parallel mirror mode occupies the region in the middle of the plot. This effect may prejudice identification of the quasi-parallel mirror mode.

The same comment might be made (to a lesser extent) about the quasi-perpendicular magnetosonic mode. Of course, one option would be to omit the quasi-parallel mirror mode as a contender (perhaps the ion acoustic mode as well) based on the fact that it is linearly damped.

One ultimate goal of this research is to use this method for large data surveys in an automated fashion. The results found here indicate that such a goal is difficult to attain. The results of our method are often probabilistic (we find the likely modes rather than a unique mode). Some of the other studies we mentioned in section 1 used a detailed analysis of polarization that may be fruitful, though as we mentioned, we are suspicious of measurements of k based on a minimum variance analysis. To get a scheme that returns a more unambiguous identification, more information may be necessary. Of course, the identification might be inherently ambiguous if there is a mixture of modes. If two or more modes are, in fact, in the plasma, it is an advantage to find that the observations match all these waves to some extent. Thus ambiguity in identification does not necessarily imply weakness of the method. It is better to have a method that yields an ambiguous result than to have one that yields an unambiguous wrong result.

6. Conclusions

We have reviewed and refined the mode identification algorithm of *Denton et al.* [1995]. Four transport ratios are used that are suitable for low-frequency ($f \ll F_{cp}$) mode identification. Table 1 gives detailed information about the theoretical values of these ratios for eight modes, the quasi-parallel and quasi-perpendicular magnetosonic, Alfvén, ion acoustic, and mirror modes. In order to get a more quantitative determination of the observed modes, we have defined a single parameter, the mode deviation D, which can be used as a measure of goodness of fit between the theoretical and observed transport ratios. Through use of the mode deviation we can find the mode that best describes the observed fluctuations; equally important, the mode deviation can be used to evaluate the uniqueness of a particular mode identification. We discuss difficulties with this method. In particular, the parallel phase ratio $R_{\parallel n_p}$ is not always well defined. *Denton et al.* [1995] showed that quasi-perpendicular mirror modes were well identified in the inner magnetosheath. Here we also identified quasi-perpendicular mirror modes in the middle magnetosheath and, in one case, Alfvén-like modes in the outer magnetosheath (making use of the cross helicity). In other cases, we showed that certain identifications were likely, Alfvén-like waves in the outer magnetosheath and mirror mode in the inner magnetosheath. The reason for ambiguity in some cases may be inhomogeity, the superposition of multiple modes, nonlinear effects, or random noise in the data.

Appendix: Extra Analysis for Event 7

Using our method, event 7 was best identified as the quasi-parallel mirror mode (section 4.3). Here we examine some further evidence, which turns out to be inconclusive.

We first decomposed the magnetic fluctuations into three components, one aligned with $\mathbf{B}_0$ and the other two orthogonal. Event 7 was observed near the magnetopause at $L = 10.5$ and LT = 1100; it was therefore near the subsolar point. The direction of $\mathbf{B}_0$ was nearly in the Y-Z GSE plane with a tilt of 50° up (positive Z) from the -Y direction. The direction in which the perpendicular (orthogonal to $\mathbf{B}_0$) magnetic fluctuations had the most power was a direction with about equal positive components of X, Y, and Z. The power of fluctuations in this direction was about twice that in the third direction. When the magnetic power was decomposed into left- and right-hand polarized components, the power was about equal in both components. This indicates that there is no pure polarization but that the perpendicular magnetic fluctuations were more nearly linearly polarized than circularly polarized.

Here we calculate the coherence C' between two fluctuating quantities F and G using a somewhat different formula for Q' than (7)

$$Q' = \frac{\sum_{i=1}^{N_{c'}} F_{\omega i} G_{\omega i}^*}{\sqrt{\left(\sum_{i=1}^{N_{c'}} F_{\omega i} F_{\omega i}^*\right)\left(\sum_{i=1}^{N_{c'}} G_{\omega i} G_{\omega i}^*\right)}}. \quad (A1)$$

where $F_{\omega i}$ and $G_{\parallel \omega i}$ are determined from an FFT of the data in the ith data segment. At each discrete frequency, the phase difference between F and G is given by the phase of Q' and the coherence C' is the magnitude of Q'. (Our definition in (7) found the coherence in phase angle without measuring the coherence of relative fluctuation amplitudes. This definition in (A1) takes both into account.) For event 7, we used $N_{c'} = 10$ data segments; this gave us a better measure of coherence than that found previously (with $N_c = 4$ in Table 2c) at the expense of worse frequency resolution. Using this definition, we found that the coherence between δn and $\delta B_\parallel$ was 0.94, with a relative phase angle of 180°. The coherence between $\delta B_\parallel$ and the perpendicular component of $\delta \mathbf{B}$ with the most power was 0.63, with a relative phase angle that was +120° for frequency f below 0.02 Hz and -120° at higher frequencies. The density was not as well correlated with the perpendicular component of $\delta \mathbf{B}$ ($C' = 0.46$). We also measured the cross helicity σ_{cp} and found it to be -0.41.

Now we discuss these results. The perpendicular fluctuations of a quasi-parallel mirror mode would be expected to be linear (with the parallel fluctuations, $\delta \mathbf{B}$ would fluctuate in a plane). The mild tendency to linear polarization found is thus consistent with the mirror mode but does not prove that the fluctuations are due to a mirror mode. The density fluctuations are best correlated with $\delta B_\parallel$, as one would expect if they are

compressed in a similar manner. For the mirror mode, we expect the parallel and perpendicular fluctuations to be correlated. They are, but one is suspicious of the significance of such a correlation, considering that the direction of $\mathbf{B_0}$ is fluctuating. (For the spin-averaged data, the maximum angle between $\mathbf{B_0}$ and our fit field (from which we determined the parallel and perpendicular components) is 14.2°. This would seem to indicate that our perpendicular and parallel components are well separated and that the correlation is meaningful. On the other hand, some averaging has already taken place to get the spin-averaged field.) The value of $\sigma_{cp} = -0.41$ is not large enough to rule out the mirror mode. In summary, these results are consistent with the observed waves being the quasi-parallel mirror mode but do not prove conclusively that they are, in fact, due to that mode.

References

Anderson, B.J., S.A. Fuselier, S.P. Gary, and R.E. Denton, Magnetic spectral signatures in the Earth's magnetosheath and plasma depletion layer, *J. Geophys. Res.*, *99*, 5877, 1994.

Belmont, G., D. Hubert, C. Lacombe, and F. Pantellini, Mirror mode and other compressive ULF modes, in *Proceedings of the 26th ESLAB Symposium, Eur. Space Agency Spec. Publ., ESA SP-346*, 1992.

Blanco-Cano, X., and S.J. Schwartz, Identification of low-frequency kinetic wave modes in the Earth's ion foreshock, *Ann. Geophys.*, *15*, 273, 1997.

Denton, R.E., S.P. Gary, B.J. Anderson, S.A. Fuselier, and M.K. Hudson, Low-frequency magnetic fluctuation spectra in the magnetosheath and plasma depletion layer, *J. Geophys. Res.*, *99*, 5893, 1994.

Denton, R.E. S.P. Gary, X. Li, B.J. Anderson, J.W. LaBelle, and M. Lessard, Low-frequency fluctuations in the magnetosheath near the magnetopause, *J. Geophys. Res*, *100*, 5665, 1995.

Denton, R.E., B.J. Anderson, G. Ho, and D.C. Hamilton, Effects of wave superposition on the polarization of electromagnetic ion cyclotron waves, *J. Geophys. Res.*, *101*, 24,869, 1996.

Gary, S.P., The mirror and ion cyclotron anisotropy instabilities, *J. Geophys. Res.*, *97*, 8519, 1992.

Gary, S.P., and D. Winske, Correlation function ratios and the identification of space plasma instabilities, *J. Geophys. Res.*, *97*, 3103, 1992.

Gary, S.P., M.E. McKean, D. Winske, B.J. Anderson, R.E. Denton, and S.A. Fuselier, The proton cyclotron instability and the anisotropy/β inverse correlation, *J. Geophys. Res.*, *99*, 5903, 1994.

Gleaves, D.G., and D.J. Southwood, Phase delays in transverse disturbances in the Earth's magnetosheath, *Geophys. Res. Lett.*, *17*, 2249, 1990.

Gleaves, D.G., and D.J. Southwood, Magnetohydrodynamic fluctuations in the Earth's magnetosheath at 1500 LT: ISEE 1 and ISEE 2, *J. Geophys. Res.*, *96*, 129, 1991.

Hubert, D., Nature and origin of wave modes in the dayside Earth magnetosheath, *Adv. Space Res.*, *14*(7), 55, 1994.

Johnson, J.R., and C.Z. Cheng, Global structure of mirror modes in the magnetosheath, *J. Geophys. Res.*, *102*, 7179, 1997.

Krauss-Varban, D., N. Omidi, and K.B. Quest, Mode properties of low-frequency waves: Kinetic theory versus Hall-MHD, *J. Geophys. Res.*, *99*, 5987, 1994.

Lacombe, C., E. Kinzelin, C.C. Harvey, D. Hubert, A. Mangeney, J. Elaoufir, D. Burgess, and C.T. Russell, Nature of the turbulence observed by ISEE 1-2 during a quasi-perpendicular crossing of the Earth's bow shock, *Ann. Geophys.*, *8*, 489, 1990.

Lacombe, C., F.G.E. Pantellini, D. Hubert, C.C. Harvey, A. Mangeney, G. Belmont, and C.T. Russell, Mirror and Alfvénic waves observed by ISEE 1-2 during crossings of the Earth's bow shock, *Ann. Geophys.*, *10*, 772, 1992.

Lacombe, C., G. Belmont, D. Hubert, C.C. Harvey, A. Mangeney, C.T. Russell, J.T. Gosling, and S.A. Fuselier, Density and magnetic field fluctuations observed by ISEE 1-2 in the quiet magnetosheath, *Ann. Geophys.*, *13*, 343, 1995.

Le, G., C.T. Russell, M.F. Thomsen, and J.T. Gosling, Observations of a new class of upstream waves with periods near 3 seconds, *J. Geophys. Res.*, *97*, 2917, 1992.

Lühr, H., N. Klöcker, W. Oelschlägel, B. Häusler, and M. Acuna, The IRM fluxgate magnetometer, *IEEE Trans. Geosci. Remote Sens.*, *GE-23*, 259, 1985.

Omidi, N., and D. Winske, Structure of the magnetopause inferred from one-dimensional hybrid simulations, *J. Geophys. Res.*, *100*, 11,935, 1995.

Papoulis, A., *Probability, Random Variables, and Stochastic Processes*, McGraw-Hill, New York, 1965.

Paschmann, G., H. Loidl, P. Obermayer, M. Ertl, R. Laborenz, N. Sckopke, W. Baumjohann, C.W. Carlson, and D.W. Curtis, The plasma instrument for AMPTE IRM, *IEEE Trans. Geosci. Remote Sens.*, *GE-23*, 262, 1985.

Paschmann, G., I. Papamastorakis, W. Baumjohann, N. Sckopke, C.W. Carlson, B.U.Ö. Sonnerup, and H. Lühr, The magnetopause for large magnetic shear: AMPTE/IRM observations, *J. Geophys. Res.*, *91*, 11,099, 1986.

Schwartz, S.J., D. Burgess, and J.J. Moses, Low-frequency waves in the Earth's magnetosheath: Present status, *Ann. Geophys.*, *14*, 1134, 1996.

Song, P., C.T. Russell, and S.P. Gary, Identification of low-frequency fluctuations in the terrestrial magnetosheath, *J. Geophys. Res.*, *99*, 6011, 1994.

Tajiri, M., Propagation of hydrodynamic waves in collisionless plasma, II, Kinetic approach, *J. Phys. Soc. Jpn.*, *22*, 1482, 1967.

R.E. Denton, J.W. LaBelle, and M.R. Lessard, Physics and Astronomy Department, Dartmouth College, Hanover, NH 03755-3528. (e-mail: richard.denton@dartmouth.edu; james.labelle@dartmouth.edu; marc.lessard@dartmouth.edu)

S.P. Gary, Los Alamos National Laboratory, Los Alamos, NM 87545. (e-mail: pgary@lanl.gov)